RESEARCH PAPER

Room temperature oxidation of Si nanocrystals at dry and wet air

Vadim M. Popelensky ⬤ **· Sergey G. Dorofeev · Nikolay N. Kononov ·**
Sergey S. Bubenov · Alexander A. Vinokurov

Abstract Oxidation of HF vapor-etched nanocrystalline silicon films, prepared by drop coating from nanocrystalline Si sol in acetonitrile, was studied. Oxidation of nanocrystalline silicon at room temperature in air with 5% and 86% relative humidity was observed by means of infrared spectroscopy for 2 days. The change in film mass after 15 h of oxidation was determined using quartz crystal microbalance. In dry air, film mass and integral intensity of bands attributed to vibrations in Si_{3-x}–Si–H_x and Si–O–Si groups changed linearly with time. In humid air, intensity of in Si_{3-x}–Si–H_x band decays exponentially and intensity of Si–O–Si band increases as a square root of oxidation time. Film mass gain after 15 h of oxidation corresponds to an average oxide layer thickness of 0.02 nm in dry air and 0.51 nm in wet air.

V. M. Popelensky · S. G. Dorofeev (✉) · S. S. Bubenov ·
A. A. Vinokurov
Department of Chemistry, Lomonosov Moscow State University,
1-3 Leninskie Gory, Moscow, Russia 119991
e-mail: dorofeev_sg@mail.ru

N. N. Kononov
Prokhorov General Physics Institute, Russian Academy of
Sciences, 38 Vavilov Str., Moscow, Russia 119991

Introduction

Nanocrystalline silicon (nc-Si) has been studied extensively for the last few years due to the possibility to use it for the production of optical (Kanemitsu 1995; Ni et al. 2019), light emitting (Gaburroa et al. 2000), and electronic (Ostraat et al. 2001; Conibeer et al. 2006) devices and biosensors (Ji et al. 2018). Silicon dioxide that is formed on the surface of silicon nanocrystals is of great importance for some other applications such as fabrication of integrated circuits.

The first studies of silicon oxidation were devoted to the thermal oxidation of monocrystalline Si (Grove and Deal, 1965, Hess and Deal, 1977, Massoud and Plummer 1985, 1987), but with a decrease of the used integrated circuits' size, the process of unprompted oxide growth on Si surface exposed to air at room temperature became more important. According to these studies, the thickness of native oxide does not exceed the size of 0.1 nm, but it has been experimentally proven (Raider et al. 1975) that after 10 h of air exposure at room temperature, the oxide layer of 1.0–1.2 nm is achieved. Therefore, it is likely that the oxidation of Si at room temperature follows a different mechanism from the one assigned to the thermal oxidation process. The oxidation of monocrystalline Si in dry oxygen, air, and ultrapure water was studied in Morita et al. (1990) and Niwano et al. (1994). These works revealed that the oxide thickness increases over time as a step-like function and that an efficient growth of oxide requires both water and oxygen. The rate of oxidation can be reduced by lowering the content of moisture in the air and oxygen in ultrapure water.

The properties of nc-Si are very different from the ones of monocrystalline Si (Koshida and Matsumoto 2003; Kovalevskii et al. 2008). The coexistence of a large number of different crystallographic planes on the surface of silicon nanoparticles, high surface curvature, and the amorphization of near-surface Si layers during the oxidation must result in a difference between oxidation kinetics for mono- and nanocrystalline silicon. Moreover, nc-Si has a much higher surface to volume ratio, which means that the effect of the surface oxide layer on the nc-Si properties is much greater in comparison with a monocrystalline Si. The oxidation of nc-Si can readily take place in air even at room temperature (Froner et al. 2006). This may make it difficult to produce an oxide film of given thickness, especially for nanometer-scale films. Therefore, for the proper use of nc-Si, we must study the process of its oxidation in air at room temperature.

As of now, several studies about the oxidation of nc-Si have already been conducted. These works feature different ambient conditions and methods of pre-oxidation treatment. Usually nc-Si are etched in HF to clean it from the initial oxide with the use of either acid or vapor etching. The change in oxide stoichiometry before etching and after etching and oxidation was reported in Pi et al. (2007), with initial oxide being the stoichiometric one and the new one appearing to be a suboxide $SiO_{1.95}$. Silicon to oxygen ratio was acquired from the Si–O–Si stretching vibration frequency shift in infrared (IR) spectra, according to the dependence from Pai et al. (1986). The change of oxygen content is attributed to the reconstruction of silicon surface after the removal of hydrogen from the surface of the etched nanoparticles (Yu et al. 2002). The decrease in photoluminescence (PL) intensity after etching and oxidation was caused by an increase in the number of defects in nc-Si, which is confirmed by the electronic spin resonance (ESR) method. It was also shown that the size of nanoparticles decreased based on PL data. Aside from simple HF etching, etching with following vacuum annealing or hydrosilylation with 1-octadecene was investigated by the means of IR spectroscopy (Niesar et al. 2012). After HF etching, Si–O–Si band disappears and Si–H appears. During oxidation, the former line returns and the latter one decays, while another Si–H band with higher frequency appears and its intensity rises over time. Annealing has no effect on oxidation, but hydrosilated nc-Si are more resistant to oxidation, as also shown by the means of DFT method

(Pi et al. 2014). It was demonstrated that oxidation of nc-Si does not proceed in dry air or degassed water at room temperature (Sprung et al. 2015), but the addition of moisture or oxygen respectively activates the process. Similar results were achieved for monocrystalline Si (Morita et al. 1990). However, the freshly prepared nc-Si are able to react with water, which was proven by the rise of Si–O–Si bonds' signal, but the growing oxide shell inhibits this reaction (Froner et al. 2006). It is supposed that adsorbed H_2O react with Si dangling bonds, and the formation of Si–OH groups polarizes adjacent Si–Si bonds to make them easier to break with the creation of another Si–OH group, which are able to form Si–O–Si bridges by condensation. Moreover, formation of oxide layer adsorbed water molecules makes it harder for O_2 species to reach the Si atoms; therefore, the oxidation rate decreases after monolayer of Si–O is formed (Melanie et al. 2014). The use of oxidizing agents' solutions ($KMnO_4$, H_2SO_4/H_2O, $K_2S_2O_8$) was researched, but the correlation between the red-ox potential and oxidation rate could not be established. The use of any of these oxidizing agents led to the complete removal of Si–H bonds from the surface of nc-Si (Litvinenko et al. 2010). The results obtained in reviewed works on nanosilicon oxidation do not contain data on the thickness of the oxide layer formed during the oxidation of nc-Si.

In this work, we studied the process of nc-Si oxidation in air at room temperature with varied humidity using IR spectroscopy and direct measurement of film mass. The latter was performed on quartz crystal resonators on which the film was deposited. Using the obtained data, we calculated the native oxide growth rate.

Experimental section

Silicon nanoparticles were synthesized by laser-induced pyrolysis of gaseous monosilane (Kuz'min et al. 2012). Nanoparticles were dispersed in acetonitrile; the the resulting sol had concentration of 3–5 mg/ml. Sol was dripped onto quartz resonators (frequency 12 MHz) in the area of one of the silver electrodes. Another blank quartz resonator was used as a comparison sample to take into account the side processes such as etching and aging of quartz crystals. Both of the resonators were opened simultaneously so that the aging processes were equal. After the deposition of nc-Si film, both quartz resonators were exposed to HF vapors for 15 min to

remove the oxidized layer of silicon, vaccum dried for 3 min in order to remove the traces of HF, and then placed into an experimental chamber with regulated humidity (see Fig. 1). The chamber was constantly purged by air with exact humidity: 5% and 86% for first and second samples respectively. The humidity was regulated by mixture of two air flows: the first one was dried by zeolite (3 Å, heated at 300 °C for 3 h), the other one was sparged through the water. The humidity was controlled by a Honeywell HIH-4000 sensor.

Films for IR studies were obtained by dripping nc-Si sol onto silver substrates and treated the same way as the ones on the quartz resonators. IR spectra were taken after certain periods of time on PerkinElmer Frontier FTIR spectrometer with Pike diffusion reflection module; blank silver substrate was used as baseline. All IR spectra were taken from the same area of nc-Si films. Si–O–Si and Si–H bands were integrated for quantitative analysis.

Relative mass change measurements of nanosilicon films upon oxidation were done on quartz crystal microbalances that worked on resonance principle. Resonant frequency measurements were performed as follows. Both resonators—with nanosilicon film and without one—were connected to two identical generators assembled according to the Kolpitz scheme; their resonant frequency was measured by two frequency meters (SANJAN STUDIO PLJ-8LED-RS) that were connected to a computer by a microcontroller made by I.Makeev. The resonant frequency-time dependence for nc-Si film was plotted, and then, the resonant frequency shift of the blank sample was subtracted. The resulting dependence was attributed only to the mass change of nanosilicon layer.

Transmission electron microscopy (TEM) was performed on a LEO912 AB OMEGA microscope (acceleration voltage: 200 kV, resolution: 0.37 nm). Size distributions of etched nanoparticles were obtained through manual calculations of nc-Si images.

Results and discussion

IR spectra evolution during the oxidation of nc-Si

IR transmittance spectra of nc-Si films deposited on silver substrate upon etching and oxidation are present on Fig. 2. Spectra (a) and spectra (b) were taken at 5% and 86% relative humidity (RH) respectively. The spectrum for initial non-etched nc-Si films is characterized by pronounced absorption band at 1240–940 cm^{-1} that conforms to various vibrational modes of Si–O–Si bonds (Weldon et al. 2000). This band almost completely disappears after 15 min of gaseous HF etching and 3 min of vacuum drying. Si–H band at 2165–2050 cm^{-1} appears because etched nc-Si are covered in Si–H bonds. Spectra taken after oxidation for 20 and 53 h show that integral intensity (further, intensity) of this Si–H band decreases upon oxidation (Fig. 3). In the case of wet air oxidation, another Si–H band at 2285–2185 cm^{-1} appears and its intensity increases with time (Fig. 4). The same Si–H band is present on the IR spectrum of the film before HF treatment because particles, synthesized by the pyrolysis of monosilane, are covered with Si–H shell and some of these bonds are still present even after continuous oxidation of these particles. The existence of Si–H shell was found in Kuz'min et al. (2012). According to literature (Falcao et al.

Fig. 1 The scheme of experimental device for nc-Si films' oxidation study. (1.a–b) quartz crystals with nc-Si films, (2) silver substrate with nc-Si film for IR studies, (3) humidity sensor, (4) electrical joints, (5) desiccant with zeolite, (6) compressor, (7) air exhaust
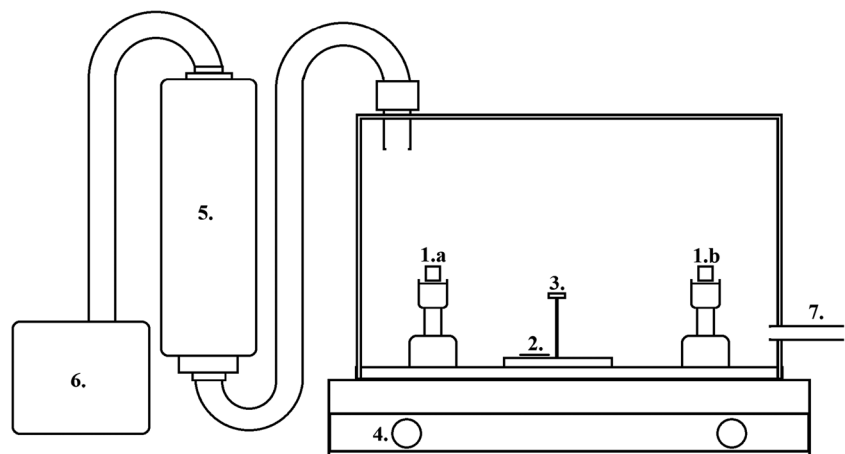
Fig. 2 (a) IR spectrum of nc-Si before and after etching in HF vapor and after 20 and 50 h of oxidation at 5% relative humidity. (b) IR spectrum of nc-Si before and after etching in HF vapor and after 20 and 50 h of oxidation at 86% relative humidity
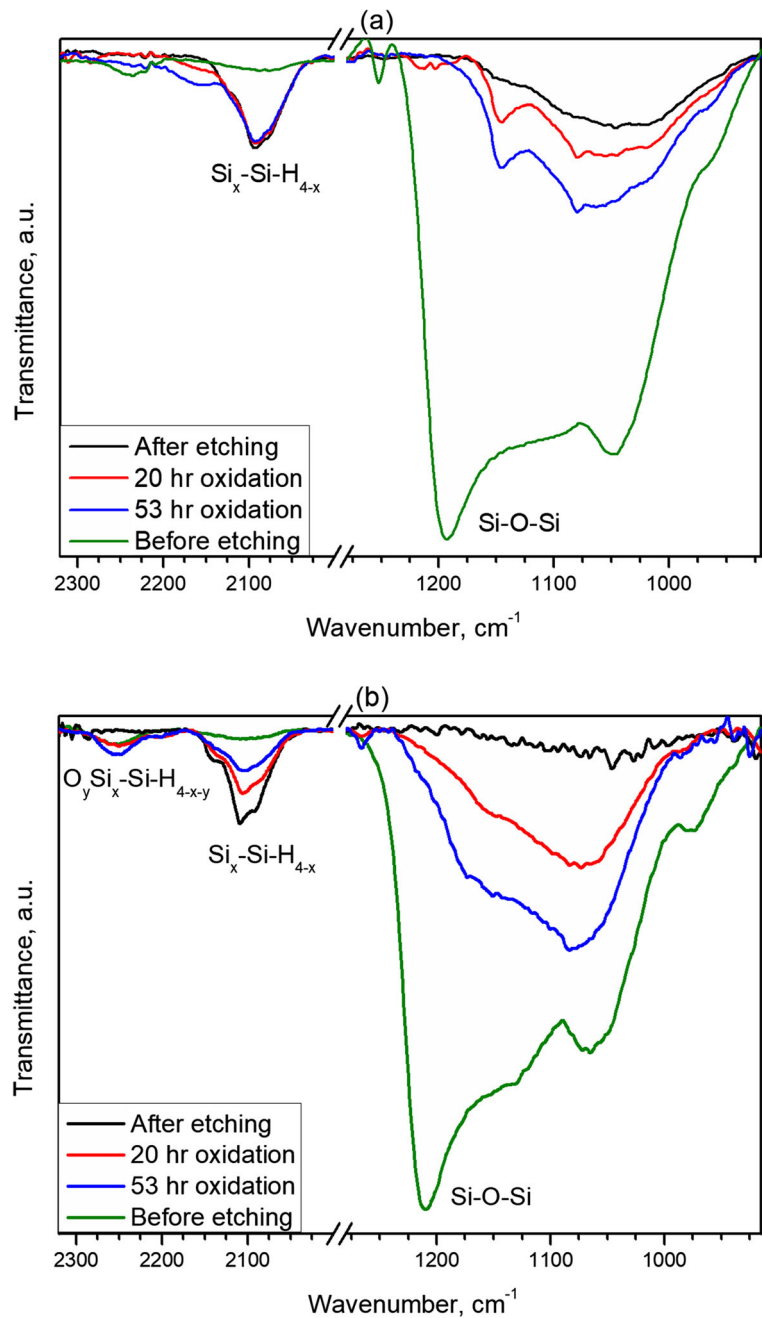
2019), the band at 2285–2185 cm^{-1} corresponds to Si–H vibrations in O_ySi_x–Si–H_{4-y-x} group in which silicon atom is bound to oxygen atom whereas the band at 2165–2050 cm^{-1} corresponds to Si–H vibrations in unoxidized H_{4-x}–Si–H_x group. Therefore, the absence of signal of O_ySi_x–Si–H_{4-y-x} group during the dry air oxidation indicates that the presence of water affects the nc-Si films' oxidation process. The initial intensity for Si–H band in H_{4-x}–Si–H_x group does not depend on RH because silicon nanoparticles are equally and completely covered with Si–H bonds after etching. Therefore, the intensities of Si–H and Si–O–Si bands on Figs. 3, 4, and 6 were normalized by initial Si–H band intensity to make it possible to compare the quantitative data. The fitting equations and adjusted R-squared are given below in Table 1 to show the fitting goodness.
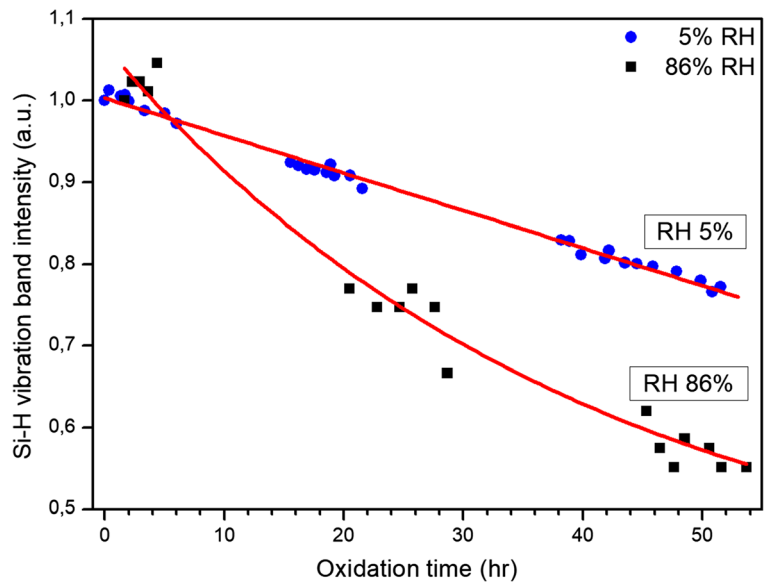
Intensities of Si–O–Si bands throughout oxidation for 5 and 86% RH are given on Fig. 5 and are proportional to quantity of oxidized silicon in the samples. In the case of high humidity, the quantity of oxidized silicon rises faster than in the case of dry air. As it can be seen from Fig. 3, the Si–H band at 2165–2050 cm^{-1} decreases faster in wet air than in dry air. It can be concluded that the rate of nanosilicon oxidation is higher in wet air than in dry air. Band for Si–H bonds can be divided in three bands as shown in Fig. 6, which allows for the better understanding of the process and shows the similarity between the oxidation of Ge and Si nanoparticles (Yuan et al. 2017). The intensity of Si–H band is the highest, which means that the majority of hydrogenated Si atoms are bond only to one H atom. During the oxidation, it becomes harder to distinguish the signals from different hydrides, though we can see

that Si–H$_3$ becomes barely noticeable which allows supposing that Si–H$_3$ groups are oxidized first.

Oxidation of nanosilicon films at high humidity (see Fig. 6) is in good agreement with the Deal–Grove model, in which the dependence of oxide thickness x on the oxidation time t is described by the following function:

$$\frac{x}{A/2} = \left[1 + \frac{t + \tau}{A^2/4B} \right]^{1/2} - 1$$

This function features parameters A, B, and τ, which are related to the physico-chemical constants of the oxidation reaction. Coefficients B and A/B are named parabolic and linear rate constants respectively, as they represent two limiting forms of the aforementioned function. Parameter τ is used to take into consideration the thickness of oxide layer formed prior to the studied
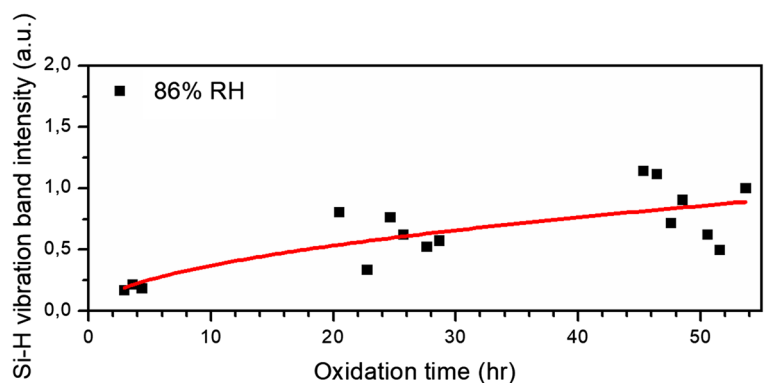
Table 1 Fitting curves for the data from Figs. 4, 5, and 6 and corresponding adjusted R^2

Group	Humidity (%)	Fitting equation	Adjusted R-squared
Si–O–Si	86	$x = 0.954 \times t^{1/2} + 1.15$	0.97644
	5	$x = 0.0445 \times t + 1.00$	0.99238
Si_{3-x}–Si–H_x	86	$x = 0.695 \times \exp(-0.0249 \times t) + 0.372$	0.97079
	5	$x = -0.00459 \times t + 1.00$	0.99347
O_ySi_x–Si–H_{4-x}	86	$x = 0.125 \times t^{1/2} - 0.0246$	0.56734

oxidation process. At oxidation times big enough to presume that $t \gg A^2/4B$ and $t \gg \tau$, the initial function is reduced to the parabolic form: $x_0^2 \approx Bt$. In the opposite situation, when the oxidation time is small and $t \ll A2/4B$, the function is reduced to linear form: $x_0 \approx \frac{B}{A}(t + \tau)$. The process consists of a fast initial oxidation stage and the following slower stage, which is also in agreement with the Deal–Grove model and also confirms the molecular dynamics calculations (Khalilov et al. 2011) and some other experimental data (Niesar et al. 2012; Melanie et al. 2014; Froner et al. 2006). Oxidation in dry air goes much slower and can be fitted with linear function, although there is a relatively small curvature during the first few hours of the oxidation. It is likely to be the result of oxidation with the participation of small quantities of water, which were adsorbed during the etching, evacuation, and transportation to the chamber with dry air. There are also constant terms in fitting equations in Table 1 that indicate the presence of traces of initial silicon oxide in etched nc-Si films, which could

have formed during evacuation in the process of removal of HF vapors after etching. Maximum of Si–O–Si band is sensitive to the stoichiometry of forming silicon oxide (Pai et al. 1986). It was found that at 86% RH, the maximum of Si–O–Si band is at 1074 cm^{-1}, whereas at 5% RH, maximum shifts to 1069 cm^{-1}. According to the dependence of oxygen content is SiO_x films on the frequency of Si–O–Si stretching vibration from Pai et al. (1986), oxidation at 86% RH leads to formation of stoichiometric oxide SiO_2, while the oxidation at 5% RH results in formation of nonstoichiometric oxide $SiO_{1.95}$.

Mass change upon oxidation

Mass change upon oxidation of nanosilicon films was studied by the means of quartz microbalances. The results are given on Fig. 7, initial masses of films are normalized to 1. IR spectroscopy (see above) demonstrates that the

Fig. 5 Integral intensities of 1240–940 cm^{-1} Si–O–Si band over oxidation time for 5% and 86% relative humidity
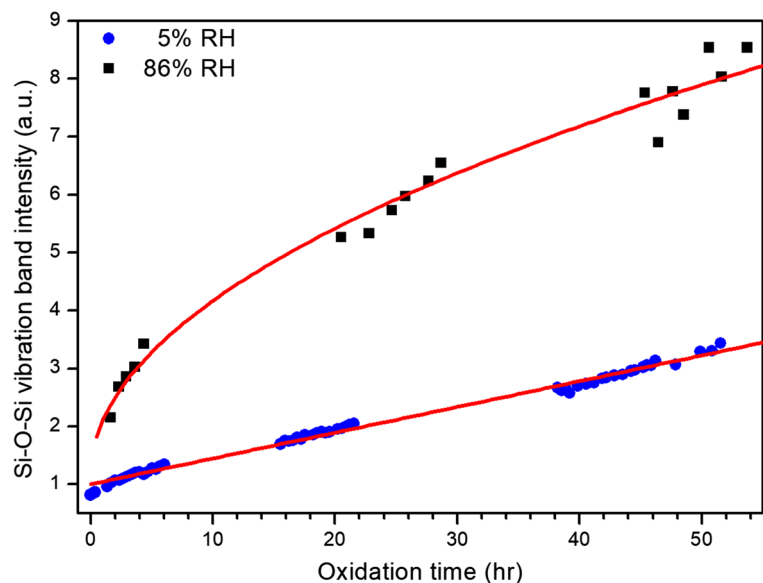
Fig. 6 The Si–H$_x$-related bands at 2030–2170 cm^{-1} were split into bands for Si–H, Si–H$_2$, and Si–H$_3$ groups
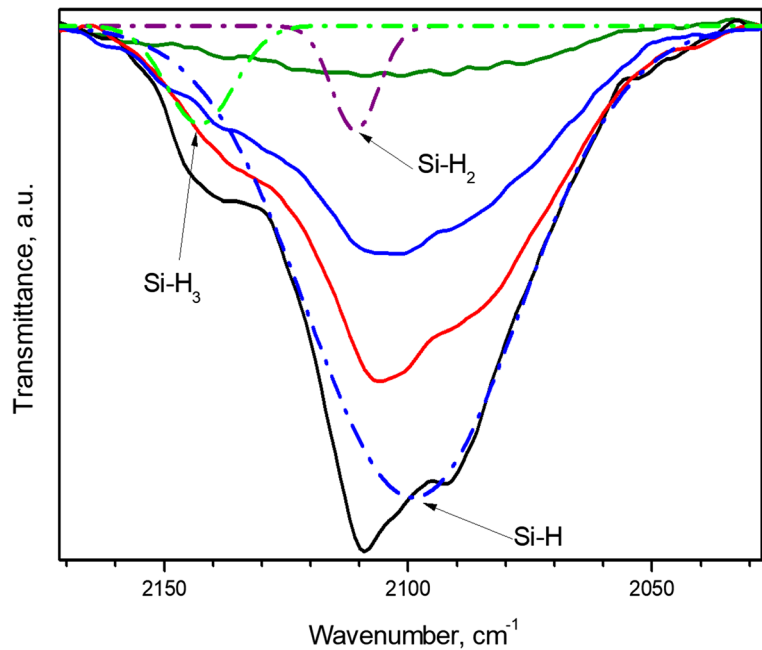

quantity of silicon oxide in nc-Si films just after the etching is low and the mass of hydrogen on the nanoparticles' surface is approximately 0.3% of film weight so it could be presumed that only the silicon determines the initial mass of nanosilicon film after etching. As can be seen in Fig. 6 at low RH, the mass change is very low (0.7%) whereas for the case of 86% RH, it rises by 38% in 15 h. At very high humidity, water can be adsorbed by the surface of silicon nanoparticles; therefore, the film was purged with dry air for 25 h to remove adsorbed water molecules. In 1 h of such treatment the film mass decreased to 124% of initial value and changes almost stopped. The final relative mass changes upon 15 h of oxidation are 0.7% and 24% for 5% and 86% RH respectively.

Low-resolution TEM image of etched nc-Si particles is given in Fig. 7 and their size distribution histogram is present in Fig. 8. Mean particle diameter is 12.9 nm (Fig. 9). Assuming that silicon nanoparticles in the films are spherical both before oxidation and after as well as taking into account the mean particle diameter after

Fig. 7 Mass change of nc-Si films over oxidation time at high (a) and low (b) relative humidity. Initial masses of films are normalized to 1. To remove adsorbed water and calculate the mass of nc-Si and its oxide, sample in (a) was purged with dry air, which is indicated by the change of RH. Dotted vertical line denotes the beginning of purging
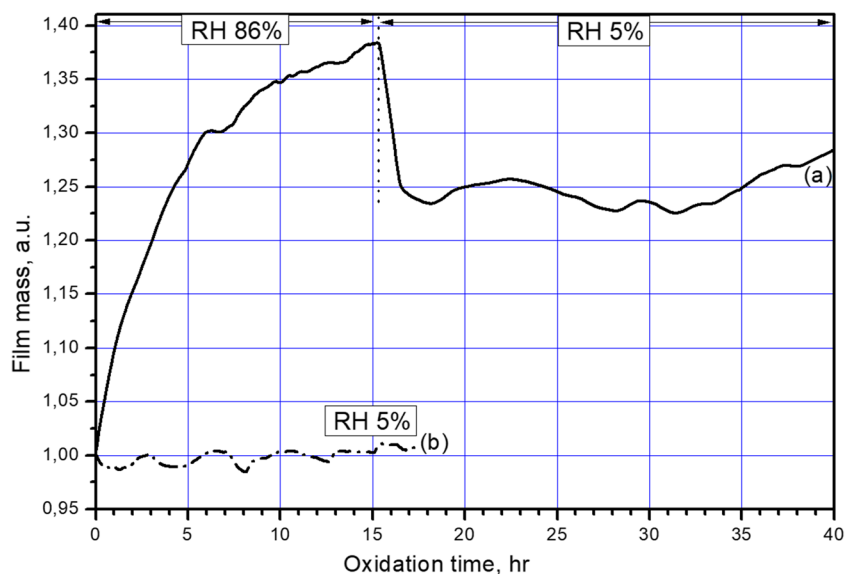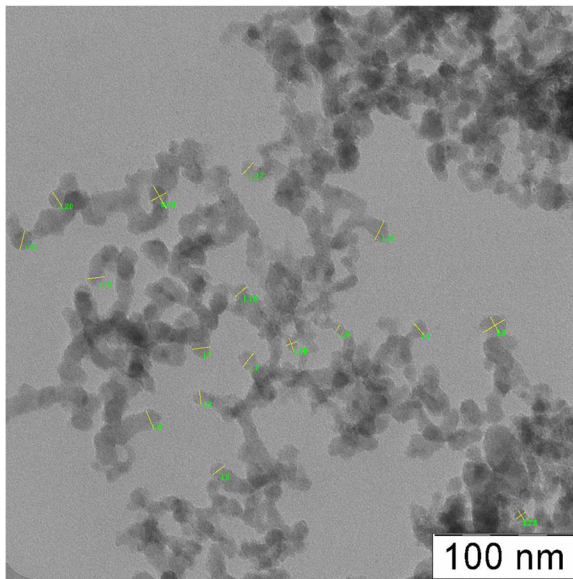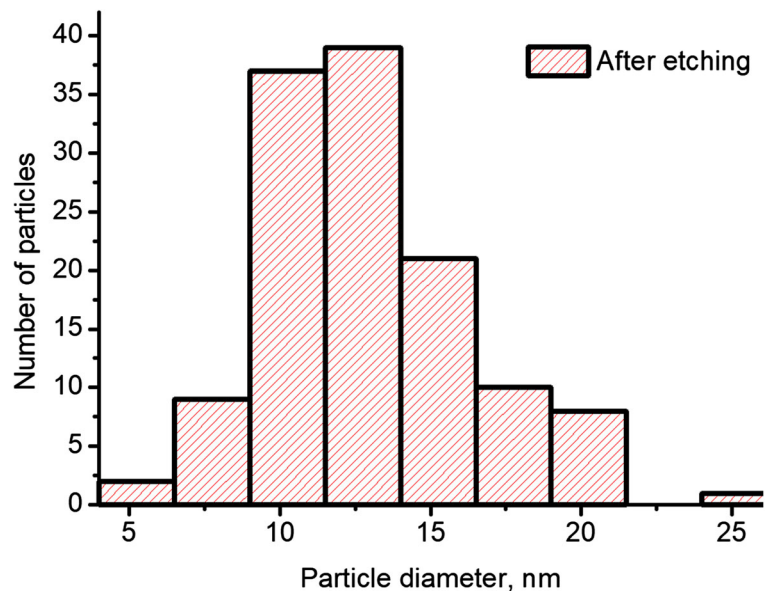
Fig. 8 TEM image of etched silicon nanoparticles. Yellow lines are some of the measurements of particles' size

etching, their relative mass change upon oxidation, and density of silicon and amorphous silica (2.329 and 2.196 g/cm^3, respectively), the thickness of oxide layer was estimated. After 15 h of oxidation, the average thickness of amorphous SiO$_2$ is 0.02 and 0.51 nm for 5 and 86% RH and the oxidation speed is approximately 0.001 and 0.034 nm/h, respectively. Since the estimated thickness of oxide that was formed in dry air is much lower than the size of one Si–O layer, it may be stated that particles are covered with oxide only partially.

Oxidation speed for the low humidity coincides with one obtained for monocrystallic silicon (Morita et al. 1990) in the same experimental conditions. We could not compare our results of nanosilicon oxidation with data on monocrystallic silicon oxidation in wet air because Morita at al. did it at 42% RH.

Conclusion

Oxidation of HF vapor-etched nanocrystalline silicon films, prepared by drop coating from nc-Si sol in acetonitrile, was studied. Oxidation of nc-Si at room temperature in air with 5% and 86% relative humidity was observed by means of IR spectroscopy for 2 days. The change in film mass after 15 h of oxidation was determined using quartz crystal microbalance. In dry air, film mass and integral intensity of bands attributed to vibrations in Si$_{3-x}$–Si–H$_x$ and Si–O–Si groups changed linearly with time. In humid air, intensity of in Si$_{3-x}$–Si–H$_x$ band decays exponentially and intensity of Si–O–Si band increases as a square root of oxidation time. Band, attributed to the Si–H vibrations in O$_y$Si$_x$–Si–H$_{4-x-y}$ group, was detected during the oxidation in humid air only and its intensity increased throughout oxidation process. Film mass gain after 15 h of oxidation corresponds to an average oxide layer thickness of 0.02 nm in dry air and 0.51 nm in wet air.

Fig. 9 Distribution of etched particles' diameter

Compliance with ethical standards

Conflict of interest   The authors declare that they have no conflict of interest.

References

Conibeer G, Green M, Corkish R, Cho Y, Cho E, Jiang C, Fangsuwannarak T, Pink E, Huang Y, Puzzer T, Trupke T, Richards B, Shalav A, Lin K (2006) Silicon nanostructures for third generation photovoltaic solar cells. Thin Solid Films 511:654–662

Falcao BP, Leitao JP, Soares MR, Ricardo L, Aguas H, Martins R, Pereira RN (2019) Oxidation and strain in free-standing silicon nanocrystals. Phys Rev Appl 11:2

Froner E, Adamo R, Gaburro Z, Margesin B, Pavesi L, Rigo A, Scarpa M (2006) Luminescence of porous silicon derived nanocrystals dispersed in water: dependence on initial porous silicon oxidation. J Nanopart Res 8:1071–1074

Gaburroa Z, Puckera G, Belluttib P, Pavesi L (2000) Electroluminescence in MOS structures with Si/SiO_2 nanometricmultilayers. Solid State Commun 114:33–37

Grove AS, Deal BE (1965) General relationship for the thermal oxidation of silicon. J Appl Phys 36:3770–3778

Hess DW, Deal BE (1977) Kinetics of the thermal oxidation of silicon O_2/HCl mixtures. J Electrochem Soc 124:735–739

Ji X, Wang H, Song B, Chu B, He Y (2018) Silicon nanomaterials for biosensing and bioimaging analysis. Front Chem 6:38

Kanemitsu Y (1995) Light emission from porous silicon and related materials. Phys Rep 263:1–91

Khalilov U, Neyts EC, Pourtois G, van Duin ACT (2011) Can we control the thickness of ultrathin silica layers by hyperthermal silicon oxidation at room temperature. J Phys Chem C 115:24839–24848

Koshida N, Matsumoto N (2003) Fabrication and quantum properties of nanostructured silicon. Mater Sci Eng R Rep 40:169–205

Kovalevskii AA, Shevchenok AA, Strogova AS (2008) Oxidation behavior of micro- and nanostructured silicon powders. Inorg Mater 44:445–449

Kuz'min GP, Kononov NN, Rozhanskii NV, Surkov AA, Tikhonevich OV (2012) The formation of nanoparticles in laser-induced SiH_4 gas reactions. Mater Lett 68:504–506

Litvinenko S, Alekseev S, Lysenko V, Venturello A, Geobaldo F, Gulina L, Kuznetsov G, Tolstoy V, Skryshevsky V, Garrone E, Barbier D (2010) Hydrogen production from nano-porous Si powder formed by stain etching. Int J Hydrog Energy 35:6773–6778

Massoud HZ, Plummer JD (1985) Thermal oxidation of silicon in dry oxygen growth-rate enhancement in the thin regime. J Electrochem Soc 132:2685–2693

Massoud HZ, Plummer JD (1987) Analytical relationship for the oxidation of silicon in dry oxygen in the thin-film regime. J Appl Phys 62:3416–3422

Melanie LM, Kenneth KC, Kristine L, Gilberto C, Geoffrey AO (2014) Size-dependent chemical reactivity of silicon nanocrystals with water and oxygen. J Phys Chem 119:826–834

Morita M, Ohmi T, Hasegawa E, Kawakami M, Ohwada M (1990) Growth of native oxide on a silicon surface. J Appl Phys 68:1272–1280

Ni Z, Zhou S, Zhao S, Peng W, Yang D, Pi XD (2019) Silicon nanocrystals: unfading silicon materials for optoelectronics. Mater Sci Eng R Rep 138:85–117

Niesar S, Pereira RN, Stegner AR, Erhard N, Hoeb M, Baumer A, Wiggers H, Brandt MS, Stutzmann M (2012) Low-cost post-growth treatments of crystalline silicon nanoparticles improving surface and electronic properties. Adv Funct Mater 22:1190–1198

Niwano M, Kageyama J, Kurita K (1994) Infrared spectroscopy study of initial stages of oxidation of hydrogen terminated Si surfaces stored in air. J Appl Phys 76:2157–2162

Ostraat ML, De Blauwe JW, Green ML, Bell LD, Brongersma ML, Casperson J, Flagan RC, Atwater HA (2001) Synthesis and characterization of aerosol silicon nanocrystal nonvolatile floating-gate memory devices. Appl Phys Lett 79:433–435

Pai PG, Chao SS, Takagi Y, Lucovsky G (1986) Infrared spectroscopic study of SiO_x films produced by plasma enhanced chemical vapor deposition. J Vac Sci Technol 4:689–694

Pi XD, Mangolini L, Campbell SA, Kortshagen U (2007) Room-temperature atmospheric oxidation of Si nanocrystals after HF etching. Phys Rev B 75:085423

Raider SI, Flitsch R, Palmer MJ (1975) Oxide growth on etched silicon in air at room temperature. J Electrochem Soc 122:413–418

Sprung C, Heimfarth J, Erler J, Ziegenbalg G, Patzold C, Singliar U, Frohlich P, Muller A, Schubert C, Roewer G, Bohmhammel K, Mertens F, Seidel J, Bertau M, Kroke M (2015) Hydrogen terminated silicon nanopowders: gas phase synthesis oxidation behavior and Si-H reactivity. Silicon 7:31–42

Weldon MK, Queeney KT, Gurevich AB, Chabal YJ, Raghavachari K (2000) Si–H bending modes as a probe of local chemical structure: thermal and chemical routes to decomposition of H_2O on Si (100)-(2×1). J Chem Phys 113:2440–2446

Pi XD, Wang R, Yang D (2014) Density functional theory study on the oxidation of hydrosilylated silicon nanocrystals. J Mater Sci Technol 30:639–643

Yu DK, Zhang RQ, Lee ST (2002) Structural properties of hydrogenated silicon nanocrystals and nanoclusters. J Appl Phys 92:7453–7458

Yuan TH, Pi XD, Yang D (2017) Nonthermal plasma synthesized boron-doped germanium nanocrystals. IEEE J Sel Top Quantum Electron 23:1–5